arXiv:cond-mat/0504533v2 [cond-mat.str-el] 2 Aug 2006

Thermodynamics of the two–dimensional Falicov–Kimball model: a classical Monte Carlo study

Maciej M. Maśka* and Katarzyna Czajka
Department of Theoretical Physics, Institute of Physics, University of Silesia, 40-007 Katowice, Poland
(Dated: March 23, 2022)

The two–dimensional Falicov–Kimball (FK) model is analyzed using Monte Carlo method. In the case of concentrations of both itinerant and localized particles equal to 0.5 we determine temperature dependence of specific heat, charge density wave susceptibility and density–density correlation function. In the weak interaction regime we find a first order transition to the ordered state and anomalous temperature dependence of the correlation function. We construct the phase diagram of half–filled FK model. Also, the role of next–nearest–neighbor hopping on the phase diagram is analyzed. Lastly, we discuss the density of states and the spectral functions for the mobile particles in weak and strong interaction regime.

I. INTRODUCTION

The study of correlated electron systems has attracted great interest over the last decades. Much of this effort was devoted to simple Hamiltonians that may contain the basic interactions to explain some properties of these systems. A common point of departure for many theoretical studies is the Hubbard model[1] which had been proposed to describe electron correlations in the narrow–band systems. This simple model has been extensively investigated over the past forty years, mostly in connection with the metal–insulator transition. After discovery of high temperature superconductors,[2] it was argued[3] that the same simple model could possibly capture some of the physics of these materials.

The Hubbard model is represented by the following Hamiltonian:

$$\mathcal{H}_{\rm Hubb} = \sum_{ij\sigma} t_{ij} c^{\dagger}_{i\sigma} c_{j\sigma} + U \sum_{i} n_{i\uparrow} n_{i\downarrow}, \qquad (1)$$

where $c^{\dagger}_{i\sigma}$ ($c_{i\sigma}$) creates (annihilates) a conduction electron with spin σ at lattice site i. The hopping integral t_{ij} is usually assumed to be non-zero for nearest neighboring sites i and j only. U is the on–site Coulomb interaction. Although at first sight such a model may seem oversimplified, only few rigorous results are known. They include the one–dimensional solution through the Bethe ansatz,[4] the Nagaoka's theorem[5] and some statements which become exact in infinity dimensions.[6,7] All other results are approximate (mostly of mean–field or perturbative type) or obtained for finite lattices, mainly by Lanczös or quantum Monte Carlo (MC) calculations.

Therefore, our starting point is a simpler model, that can be viewed as a limiting case of a generalized (asymmetric) Hubbard model. In the original Hubbard Hamiltonian (1) the hopping integral t is spin independent. However, one can assume that the mass of spin–up and spin–down electrons are different, and in the limit of infinitely massive spin–down electrons, they localize and only spin–up ones occur in the first sum in Eq. (1). Such an approximation to the Hamiltonian (1) was already used by Hubbard.[1]

Denoting $c^{\dagger}_{i\uparrow}$ ($c_{i\uparrow}$) by $c^{\dagger}_{i}$ (c_i), $n_{i\uparrow}$ by n_i and $n_{i\downarrow}$ by w_i, the resulting Hamiltonian reads

$$\mathcal{H} = -t \sum_{\langle ij \rangle} c^{\dagger}_{i} c_{j} + U \sum_{i} n_i w_i. \qquad (2)$$

Here, w_i is equal to 0 or 1, according to whether the site i is occupied or unoccupied by a massive particle. The Hamiltonian (2) is known as the FK Hamiltonian.[8] Within the framework of a common interpretation of the FK Hamiltonian, there are two species of particles: itinerant electrons and classical localized particles. The classical particles have various physical interpretations: localized (f) electrons, spin–down electrons, ions, impurities, nucleons. In the following we refer to them as "ions". The ions interact on–site with electrons. There are no direct interactions neither between the electrons nor between the ions. However, the electron–ion Coulomb interaction leads to an effective interaction between ions. As a result, for a given number of ions, the ground state energy depends on their distribution.

The FK model has a long and successful history in dealing with correlated electron systems. Introduced in 1969 to describe the metal–semiconductor transition in SmB_6 and related materials,[8] has been also studied as a model of crystallization due to effective interactions mediated by band electrons,[9,10] as a binary alloy model and many others. The FK model is also useful for describing systems that exhibit a phase separation[11,12,13,14,15] and stripe formation.[16,17,18]

The FK Hamiltonian is over thirty five years old, or even older if one takes into account that Hubbard used it in 1963 as an approximation to his model. However, while it is simpler than the Hubbard model, the general solution is also not known. On the other hand, there is much more rigorous results for the FK model, then for the Hubbard one. One of the most important, proved by Kennedy and Lieb,[9,10] says that at low enough temperature the half–filled Falicov–Kimball model possesses a long range order, i.e., the ions form a checkerboard pattern, the same as in the ground state. It is a phase, where the lattice can be divided into two interpenetrating sublattices A and B in such a way, that all nearest neighbors

of a site from sublattice A belongs to sublattice B and *vice versa* and ions occupy only one of them. This result holds for arbitrary bipartite lattices in dimensions $d \geq 2$ and for all values of the interaction strength U. Apart from this result not very much is known about solutions for two–dimensional systems.[16,19,20] Most of other results for the FK model concern one–dimension case[21,22,23,24] or the infinite–dimensional limit.[25,26] The present interest in this model was renewed in connection with developing new calculation methods that can be applied to the FK model. In particular, the dynamical mean–field theory[27] (DMFT) provides the exact solution of the FK model in infinite dimensions.[25,26] While it is known that the DMFT captures many key features of the FK model even in finite dimensions, this approach also has some limitations. The local approximation used in the DMFT does not allow to incorporate any nonlocal correlations, which are necessary to describe many of phases that are expected to realize in the FK model. An extension to the DMFT that include short–range dynamical correlations has been recently proposed.[28,29] Within this approach, called dynamical cluster approximation (DCA), the "impurity" used in the DMFT is replaced by a finite–size cluster.

At non–zero temperature the partition function has to be calculated for each ionic configuration, and then one has to average over the configurations ("annealing"). However, since the number of ionic configurations increases very rapidly with the size of the system, such a procedure is possible in some cases only. One of them is called "restricted phase diagram" method,[19] where only periodic configurations on infinite lattice are taken into account. In order to include *all* possible configurations, one has to significantly restrict the size of the lattice. In such a case an exact diagonalization technique can be applied.[30] This approach is particularly useful for low–dimensional systems, where the finite size effects are of relatively small importance. Moreover, for linear chains it is possible to perform $N \to \infty$ extrapolation in a systematic way. On the other hand, it is difficult to perform the exact diagonalization studies at finite temperatures. In order to calculate the partition function one has to run a summation over 2^N ionic configurations. Therefore, the maximum size of the clusters suitable for exact diagonalization study is strongly limited. In Ref. 30 the largest clusters consisted of 24 lattice sites.

In the present contribution we propose to avoid these limitations by using the MC method, where thermodynamic quantities for the FK model are determined by sampling the ionic configuration space stochastically. This approach allows us to investigate clusters of up to a few hundred sites. Since the frozen particles are classical ones, we do not have to use the quantum MC algorithm with the "fermionic sign" problem, and thus the calculations are not restricted to the high–temperature regime.

The present calculations are restricted to the neutral half–filled case, where the number of ions is equal to the number of electrons and their sum is equal to the number of lattice sites. The developed formalism can be straightforwardly used away from half–filling, however, the computational effort in this case is much larger, mainly due to the richness of the zero-temperature phase diagram of the FK model. Nevertheless, some results for various concentrations have already been obtained.[31]

The present simulations are performed on a square lattice. However, also in this aspect the generalization to other geometries is straightforward.[32]

The outline of the paper is as follows. Section II describes the formalism. In particular, it is demonstrated there how the classical Metropolis algorithm can be adopted to a system with both classical and quantum particles. In Section III, we analyze the order–disorder phase transition, especially in the small–U regime. It was suggested in Ref. 33 that in this regime the FK model exhibits a first order phase transition. Here, we analyze this possibility in detail. Section IV is devoted to the dependence of the phase–transition–temperature on the interaction U. Using temperature dependence of the specific heat and charge density wave (CDW) susceptibility we identify the critical temperature, constructing a phase diagram in the $T - U$ plane. In Section V, we demonstrate how the long range order vanishes when the temperature increases. Its temperature dependence is anomalous in a small–U limit. Section VI is devoted to the ground state and the phase diagram of the FK model with next–nearest–neighbor hopping. Section VII presents the results for the density of states and spectral functions of the mobile particles. Section VIII contains our conclusions.

II. COMPUTATIONAL METHOD

In all simulations we have used the Metropolis algorithm.[34] Our system contains classical (ions) as well as fermionic (electrons) degrees of freedom. The appropriate way to treat such a Hamiltonian is to define the grand canonical partition function as

$$\mathcal{Z} = \sum_{\mathcal{C}} \mathrm{Tr}_e e^{-\beta\left[\mathcal{H}(\mathcal{C}) - \mu\hat{N}\right]}, \tag{3}$$

where $\mathcal{H}(\mathcal{C})$ is the Hamiltonian (2) for a fixed ionic configuration $\mathcal{C}$, $\sum_{\mathcal{C}}$ indicates summation over ionic configurations, Tr_e denotes the trace over fermionic degrees of freedom, β is the inverse temperature, and $\hat{N}$ is the operator for the total number of electrons. For a given ionic configuration the Hamiltonian $\mathcal{H}(\mathcal{C})$ can be diagonalized numerically and the summation over fermionic degrees of freedom gives the partition function in the following form

$$\mathcal{Z} = \sum_{\mathcal{C}} \prod_{n} \left\{ 1 + e^{-\beta[E_n(\mathcal{C}) - \mu]} \right\}, \tag{4}$$

where $E_n(\mathcal{C})$ are eigenvalues of $\mathcal{H}(\mathcal{C})$. Introducing the electronic free energy

$$\mathcal{F}_e(\mathcal{C}) = -\frac{1}{\beta}\sum_n \ln\left\{1 + e^{-\beta[E_n(\mathcal{C})-\mu]}\right\}, \qquad (5)$$

the partition function can be written in a form analogous to that used for a spin system

$$\mathcal{Z} = \sum_{\mathcal{C}} e^{-\beta\mathcal{F}_e(\mathcal{C})}. \qquad (6)$$

The above equation describes the effective model, that results from the summation over the fermionic degrees of freedom. As the electronic free energy $\mathcal{F}_e(\mathcal{C})$ depends on temperature, the corresponding Hamiltonian, describing only the classical particles would include temperature–dependent interaction. This dependence may lead to nontrivial critical exponents. Equation (6) indicates also, that in the Metropolis algorithm we should use the electronic free energy in the statistical weights. To do this, however, one has to know the value of the chemical potential μ, and apart from specific cases (e.g., half–filling) it has to be determined separately. Since the calculations are carried out in the grand canonical ensemble, the chemical potential must be kept constant during the simulation. Determining thermodynamic quantities, the averages are calculated with the statistical weights

$$w(\mathcal{C}) = \frac{1}{\mathcal{Z}} e^{-\beta\mathcal{F}_e(\mathcal{C})}, \qquad (7)$$

of corresponding ionic configurations $\mathcal{C}$.

One of the advantages of the proposed approach is that it gives densities of states and spectral functions for the mobile particles that identically satisfy different sum rules. This will be discussed in Sec. VII.

The calculations were carried out on clusters up to 10^4 lattice sites, however, in most cases square clusters 20×20 were used. Usually, the simulations started at high temperature, with the initial state with randomly distributed ions. Then, the temperature has been slowly decreased. Below some temperature, ions started to form a checkerboard patterns.

It is difficult to describe the process of pattern formation qualitatively. In some cases it is convenient to use $\Delta \equiv |\langle n_A\rangle - \langle n_B\rangle|$, where $\langle n_A\rangle$ ($\langle n_B\rangle$) is the ion concentration in sublattice A (B), as the order parameter. However, such a description is not well suitable for cluster calculations, since even in the case, when in the ground state ions form almost perfect checkerboard, Δ can be close to zero. Figure 1 presents an example of such a ionic configuration. A small staggered field can be introduced in order to prevent an occurrence of such effects. However, this "phase smoothing out" may restrict also some other configurations.

Instead, we use the density–density correlation function for the ions to describe the ordered state. It has the advantage that it is capable to describe long range as well as short range correlations. We define the correlation function in the following way:

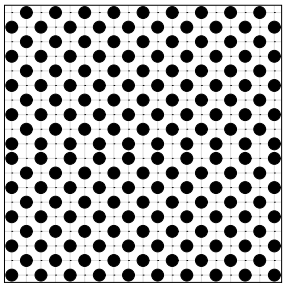


FIG. 1: Example of almost perfect checkerboard ionic configuration, for which the long range order parameter Δ is close to zero. Filled circles represent sites occupied by the massive particles.

$$g_n = \frac{1}{4N}\sum_{i=1}^{N}\sum_{\tau_1,\tau_2=\pm n} w(\boldsymbol{r}_i)\, w(\boldsymbol{r}_i + \tau_1\hat{x} + \tau_2\hat{y}), \qquad (8)$$

where $w(\boldsymbol{r}_i) \equiv w_i$, $\hat{x}$, and $\hat{y}$ denotes unitary vectors along the x and y directions, respectively (the lattice constant $a = 1$ has been assumed). Note, that g_n describes correlations along the lattice axes.

The correlation function g_n describes ionic configuration only. However, the distribution of the light particles correlates with the ionic distribution due to the direct interaction between these two types of particles. The larger value of U the stronger correlations take place. Figure 2 demonstrates these correlations for weak (upper configurations) and strong (lower configurations) interaction.

If there is a phase transition, some thermodynamical quantities have to diverge at the critical temperature. Here, we used the CDW susceptibility χ and the specific heat C_V to determine this point. The CDW susceptibility is related through the fluctuation–dissipation theorem to the variance of the density–density correlation function. This is a form especially convenient for the MC calculations

$$\chi = \frac{1}{k_{\mathrm{B}}T}\left(\langle g_1^2\rangle - \langle g_1\rangle^2\right), \qquad (9)$$

where we used $\langle\ldots\rangle$ to indicate the average over generated ionic configurations. It is a little bit more complicated to determine the specific heat. Within the standard MC approach the specific heat is calculated from the fluctuations of the energy, similarly to Eq. (9). In our case, however, according to Eq. (7) we use the electronic free energy in the Metropolis algorithm and the internal energy is not directly available from the simulations. On the other hand, the Fermi energy is much larger than the order–disorder transition temperature. Therefore, estimating the specific heat we replace the trace over the fermionic degrees of freedom by a ground state expectation value E,[35] which is a temperature–independent

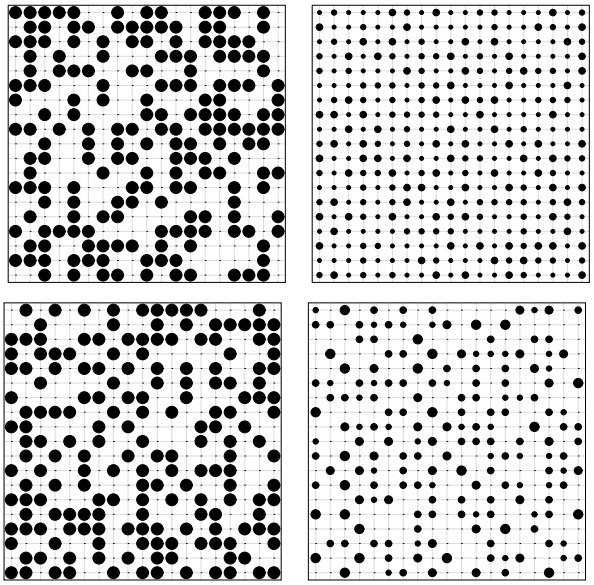


FIG. 2: Examples of ionic (left) and electronic (right) configurations for weak ($U/t = 0.5,\ k_{\rm B}T/t = 0.1$, upper row) and strong ($U/t = 5,\ k_{\rm B}T/t = 0.3$, lower row) interaction. Diameters of the circles in the right configurations are proportional to the concentration of electrons.

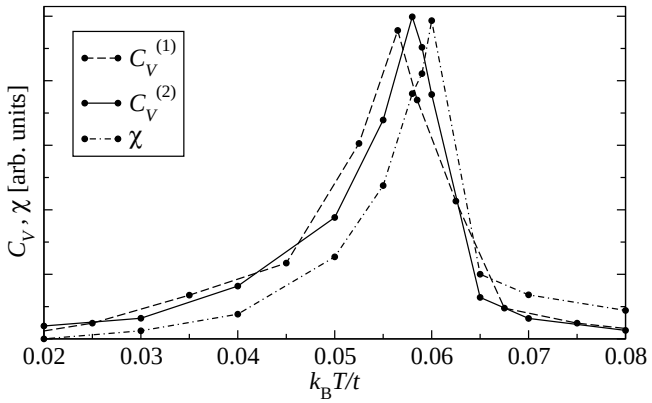


FIG. 3: Specific heat determined from Eq. (10) ($C_V^{(1)}$, dashed line) and from Eq. (11) ($C_V^{(2)}$, solid line) for $U/t = 1$. For comparison, CDW susceptibility χ is also presented (dashed–dotted line).

quantity. Then, the specific heat can be determined from the fluctuation–dissipation theorem

$$C_V = \frac{1}{N}\frac{1}{k_{\rm B}T^2}\left(\langle E^2\rangle - \langle E\rangle^2\right). \qquad (10)$$

In order to confirm the validity of this approximation we compare the specific heat determined numerically from the relation

$$C_V = \frac{dU}{dT} \qquad (11)$$

and that from Eq. (10). Since the simulations were carried out only for a given set of temperatures, a finite difference approximation had to be used for the derivative in Eq. (11). Nevertheless, within the temperature regime of interest the difference is below a few percent. Figure 3 shows a comparison of the specific heat calculated from Eq. (10) and from Eq. (11). Additionally, the CDW susceptibility is plotted there in order to indicate the critical temperature. A comparison of the critical temperatures determined from the specific heat and from the CDW susceptibility, presented in Figs. (10–12), confirms the validity of the proposed approach as well. Note, that these quantities are calculated in completely different ways: the specific heat is determined from the eigenvalues of the fermionic Hamiltonian, whereas the CDW susceptibility from the correlation function of the classical particles.

In each simulation the ensemble averages of the thermodynamic quantities of interest are calculated after the system equilibrated. The thermalization period varies with temperature. In particular, it is very long at low temperatures or in the vicinity of critical points (the critical slowdown). In order to determine whether the system has reached equilibrium, we usually start the simulation with two replicas of the system: one starting from a fully ordered state, the other from a random ion distribution. Then, the energies of the systems evolve crossing each other after some number of MC steps. This point is considered as the beginning of equilibrium state and the averages of the thermodynamic quantities are calculated over the remaining MC steps. This procedure is especially useful close to the transition temperature.

The width of the peak in the specific heat and in the CDW susceptibility decreases with the increase of the size of the system and a finite–size scaling should be carried out in order to determine precisely the transition temperature. This can be done, for instance, using the standard Binder cumulant method.[36] However, taking into account the huge amount of time needed to run the finite–size scaling over the whole parameter space, we have decided to omit to do it and most of the presented results have been obtained for 20×20 cluster. Such a cluster is sufficiently large to produce results accurate enough to describe the properties of the model under investigation and, on the other hand, the time of a single simulation run is short enough to allow determination of the full phase diagram. Moreover, some comparison of results obtained for 20×20 and 40×40 clusters is presented in Section VII.

III. NATURE OF THE PHASE TRANSITION

For large U there is an Ising–like phase transition at the critical temperature $T_c \propto U^{-1}$. In the small–U regime the critical temperature is bounded from below by $U^2/|\ln U|$.[9,10] In fact, it was shown that in large dimensions $T_c \propto U^2|\ln U|$ for $U \to 0$.[26]

It is known that for large U the Falicov–Kimball model

belongs to the same universality class as the Ising model and the order parameter is described by Curie–Weiss law $\Delta = \tanh(\Delta/\Theta)$, where $\Theta = T/T_c(U)$. Thus, the phase transition is of second order in this regime. On the other hand, it was shown in Refs. 26 and 37, that in infinite dimensions in the small–U limit the order parameter has a strange non–BCS–like temperature dependence. Therefore, it is important to determine precisely the nature of the phase transition in this regime. We have used a method proposed by M. Challa *et al.*[38] to distinguish between first and second order phase transitions. Systems undergoing first order phase transitions are accompanied by free energy barriers which separate the free energy minima characterizing the coexisting phases. It results in discontinuities in the first derivatives of the free energy, e.g., the internal energy. This, in turn, leads to a δ–type singularity in the specific heat at the transition.

Within the framework of Metropolis MC approach the energy E fluctuates with the probability distribution $P(E)$ usually given by a Gaussian. Its width is proportional to the specific heat. However, if the system is close to the first order transition, the probability distribution $P(E)$ is a superposition of two Gaussians centered at different energies, E_+ and E_-. Here, E_+ and E_- are the energies in the high– and low–temperature phases, respectively. The Gaussians are weighted by the Boltzmann factors of E_+ and E_-, and thus this splitting occurs in a vicinity of the transition temperature only. At higher (lower) temperatures $P(E)$ forms a single Gaussian centered at E_+ (E_-).

Figure 4 shows the energy distribution for temperatures slightly below and above the transition temperature for $U/t = 0.5$. Since the data has a double–peak structure, the phase transition is of the first order. One can see the transfer of the weights from the low–temperature Gaussian peak (the lower panel in Fig. 4) to the high–temperature one (the upper panel), as the temperature increases, passing through the critical value. The energy distribution at the critical point, where the heights of both the peaks are comparable, has been presented in Ref. 33.

At temperatures much lower and much higher than the transition temperature, the energy distribution can be well fitted by a single Gaussian. Such situations are presented in Fig. 5.

The energy distribution at low temperature (lower panel in Fig. 5) consists of a large number of peaks, clearly visible in the inset. They are connected with the discrete spectrum of the Hamiltonian for a finite system. Namely, at such a low temperature, there are only a few dislocations in the checkerboard ionic configuration. Due the low concentration of the dislocations, they are almost independent and each of them changes the energy by an approximately the same amount. In this way, two successive peaks correspond to configurations with the numbers of dislocations that differ by one. As the number of dislocations increases, they start to "feel" each other, and the effective interactions smear out this energy ladder. This is why the peaks are visible only in the low–energy part of the distribution. Of course, when the size of the lattice increases, the energy spectrum becomes quasicontinuous and the oscillations disappear.

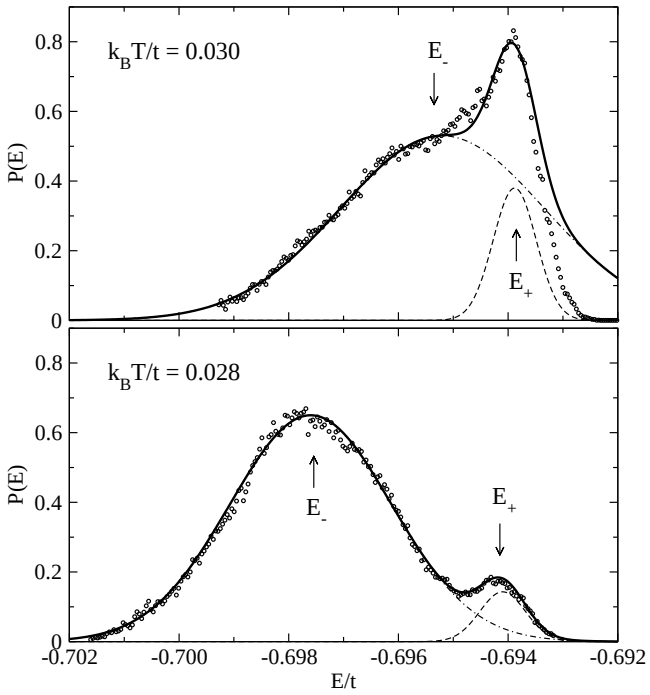


FIG. 4: Probability distribution of the energy at temperatures close to the critical temperature for $U/t = 0.5$. The thick solid lines represent a superposition of two Gaussians that fit the simulation results, whereas the dashed and dashed–dotted lines show the component Gaussians. The arrows indicate positions of the centers of the Gaussians representing low–temperature (E_-), and high–temperature (E_+) phases, respectively.

The coexistence of low– and high–temperature phases at the phase transition can also be observed in the CDW susceptibility. Fig. 6 shows the two–peak structure of the probability distribution of χ. It should be noted that the distribution presented in Fig. 6 describes ionic configurations, whereas the one presented in Fig. 4 is obtained from the eigenvalues of the fermionic Hamiltonian. The similarity between these two distributions speaks strongly in favor of the validity of the proposed MC approach, confirming the presence of first order phase transition in the small–U regime.

The magnitude of splitting of the energy distribution close to T_c decreases with the increase of the interaction strength U and above a critical value U^* disappears. The same holds true for the distribution of the CDW susceptibility. Figure 7 presents the energy and CDW susceptibility distribution at the phase transition for $U/t = 3$. One can notice an excellent agreement with the theoretical Gaussian curve, indicating an absence of any phase coexistence and the second order character of the phase transition.

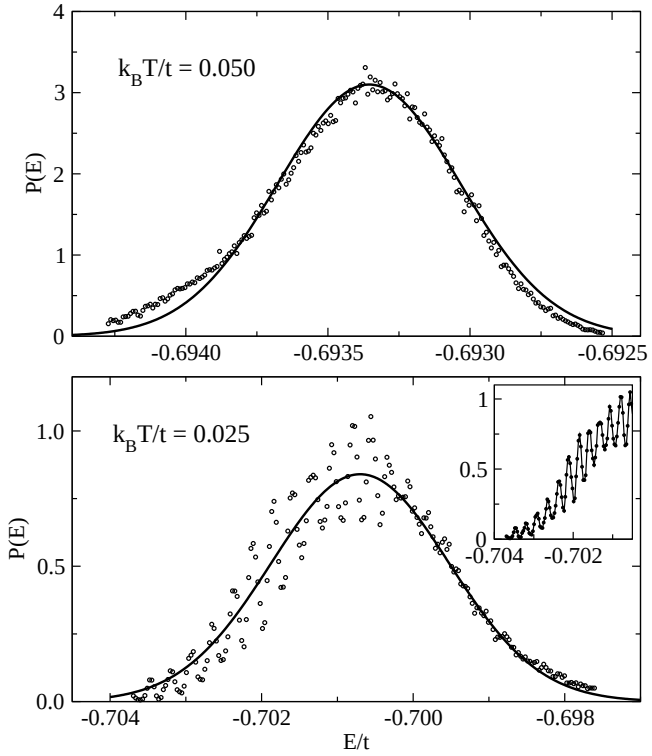


FIG. 5: Probability distribution of the energy at temperatures much higher and much lower than the transition temperature for $U/t = 0.5$. Inset in the lower panel shows the low–energy part of the distribution with lines connecting the points.

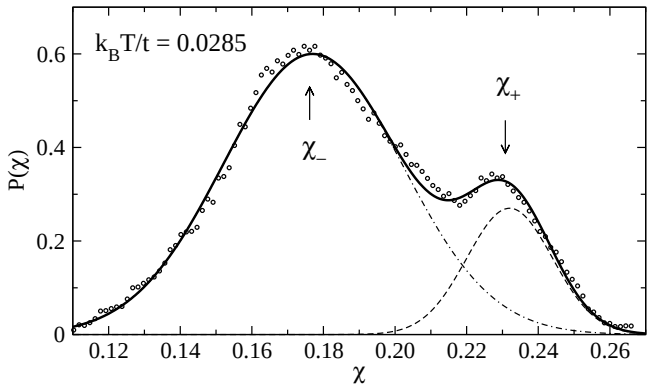


FIG. 6: Probability distribution of the CDW susceptibility χ close to the phase transition for $U/t = 0.5$. The meaning of the lines is analogous to that of Fig. 4.

We have estimated the critical value $U^* \approx t$, however, extensive numerical studies are necessary in order to determine U^* precisely.

A. Phase diagram

The position of peaks in the specific heat and the CDW susceptibility has been used to determine the critical temperature. Fig. 3 shows the typical temperature dependence of the specific heat. The phase diagram has been constructed using results obtained for 20×20 system. Figure 8 presents the transition temperature as a function of the interaction strength. The horizontal axis is plotted as $U/(U+t)$, such a scaling allows one to present both the weak and strong coupling results in the same graph. There are also shown results obtained by means of other methods: DMFT for $d = \infty$ case, taken from Ref. 37, MC taken from Ref. 20, and DCA taken from Ref. 28. In the large–U limit the critical temperature for the Ising model is also presented for comparison.

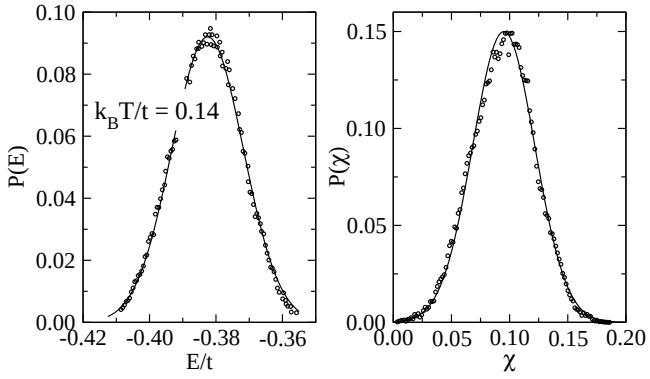


FIG. 7: Probability distribution of the energy (left panel) and of the CDW susceptibility (right panel) at the phase transition for $U/t = 3$.

IV. ORDER PARAMETER

In order to quantitatively describe the ionic configuration, we have investigated the density–density correlation function defined in Eq. (8). This function is capable of descring short range as well as long range order. In a fully ordered (checkerboard) state it oscillates with a period equal to two lattice constants (see Fig. 9).

It is convenient to define a renormalized correlation function $G_n = (-1)^n 4\left(g_n - \rho_i^2\right)$, $\rho_i \equiv N_i/N$ is the concentration of ions, where N and N_i are numbers of lattice sites and ions, respectively. Such a function is equal to 1 for the checkerboard state and close to 0 for randomly distributed ions, independently of the distance n (for $n > 0$). Apart from these limiting cases, this function decreases monotonically with increasing distance. Figures 10–12 present the temperature dependence of G_n for a wide range of the interaction U. These curves are presented together with the temperature dependencies of the specific heat and the CDW susceptibility, calculated for the same values of U. This allows one to find the exact values of the critical temperatures.

For strong to intermediate values of the Coulomb interaction there is a distinct peak in the specific heat, indicating the phase transition from the ordered state to the disordered one. The corresponding vanishing of the

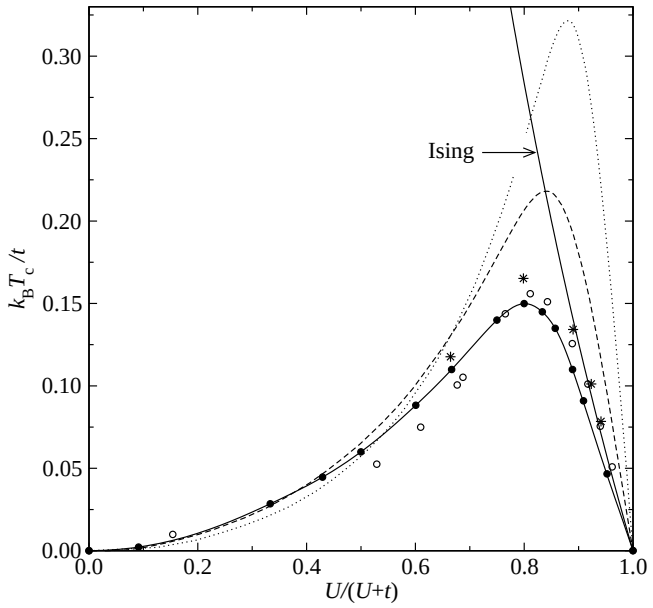


FIG. 8: Transition temperature for the $d = 2$ half–filled Falicov–Kimball model as a function of the interaction strength (solid line with circles). The dotted and dashed lines present for comparison results taken from Ref. 37. These results were obtained in $d = \infty$ limit for the Bethe lattice (dotted line) and the hypercubic lattice (dashed line). Open circles represent numerical results taken from Ref. 20, estimated as the temperature at which a gap in the density of states closes. Stars represent results obtained in Ref. 28 from DCA with a QMC for a 36-cite cluster. The solid line connecting filled circles is a guide for the eyes only.

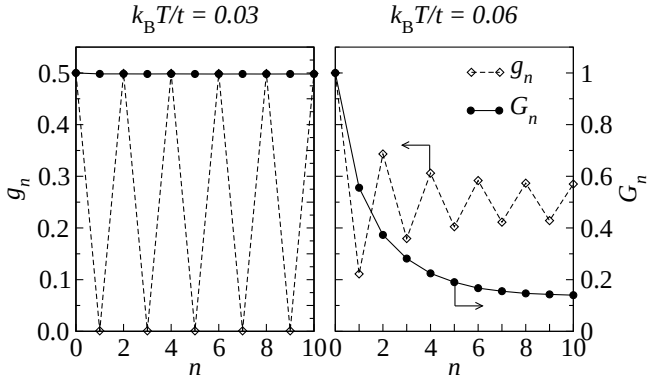


FIG. 9: Correlation functions g_n (dashed lines) and G_n (solid lines) for $U/t = 20$. Left panel shows the case of a fully ordered (checkerboard) state and the right one corresponds to the vicinity of the phase transition.

correlation function G_n resembles a typical behavior of an order parameter close to the second order phase transition (see Figs. 10 and 11). Note, that the long range correlations disappear more rapidly than that for shorter distances. This can be, however, attributed to the finite size of the system.

On the other hand, in the weak interaction limit

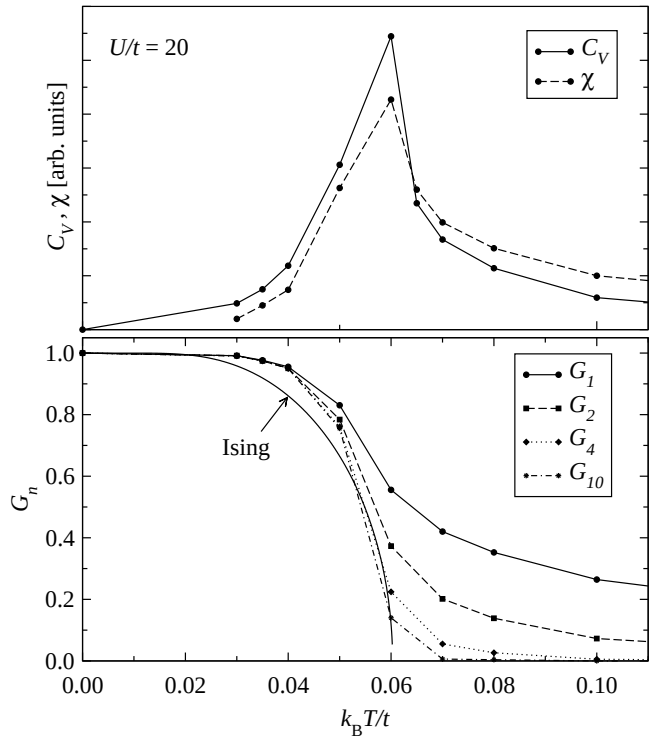


FIG. 10: Specific heat C_V and CDW susceptibility χ (upper panel) and correlation function G_n (lower panel) as a function of temperature for $U/t = 20$. Various lines in the lower panel correspond to correlation functions G_n calculated for various distances n. For comparison, there is also a line representing temperature dependence of the magnetization in the Ising model

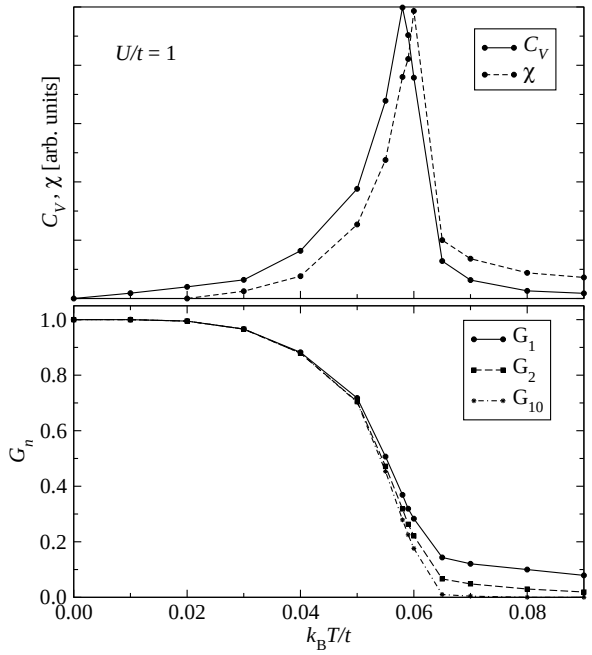


FIG. 11: The same as in Fig. 10 but for $U/t = 1$.

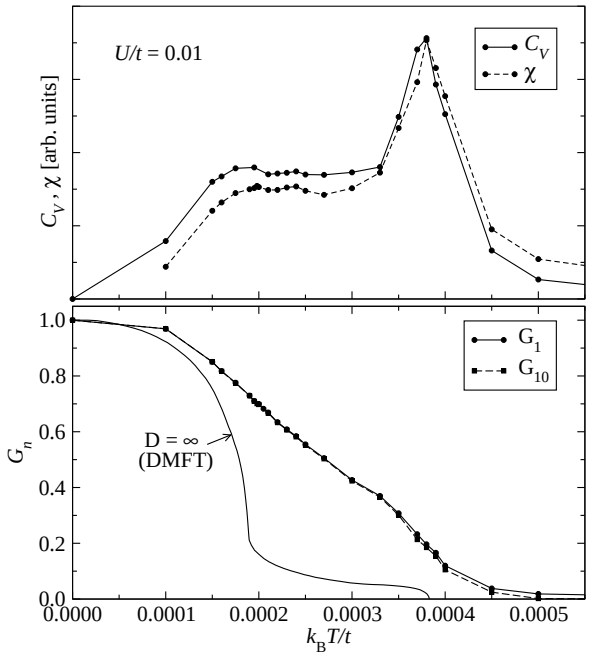


FIG. 12: The same as in Fig. 10 but for $U/t = 0.01$. Additionally, there is also a line representing the order parameter determined from DMFT solution of the FK model in infinite dimensions in the limit $U \to 0$. This solution is taken from Ref. 39.

the correlation functions vanishes almost linearly and the slope begins already at temperature approximately $0.25T_c$. An unusual behavior in this regime is seen also in the specific heat: there is hump in both $C_V(T)$ and $\chi(T)$ close to the temperature at which the slope in $G_n(T)$ occurs. Fig. 12 illustrates such a behavior for $U/t = 0.01$. For weaker interaction the values of the specific heat and the CDW susceptibility are different, however, the shape of their temperature dependence, as well as the temperature dependence of the correlation function, remain almost unchanged.

Such an anomalous temperature evolution of $G_n(T)$ may be explained as a result of finite size of the system. For small values of U there exist solutions with periodic ionic configurations possessing very large period. Such configurations are excluded from our calculations due to limited size of the clusters the simulations were carried out on.

On the other hand, it was recently shown that similar behavior of the order parameter occurs in the infinite–dimensional limit.[37,39] Our results may suggest that such a behavior is a generic property of the weak–coupling Falicov–Kimball model.

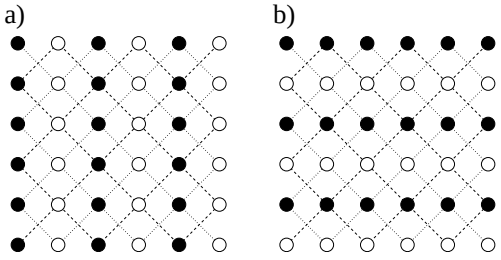


FIG. 13: Possible ground–state ionic configurations in $t' \gg t$ limit. The dashed and dotted lines indicate (independent in $t \to 0$ limit) sublattices.

V. NEXT–NEAREST–NEIGHBOR HOPPING

A. Ground state

In this section we generalize the FK Hamiltonian by taking into account the hopping to next nearest neighbors (NNN) with the hopping integral t' in addition to the nearest–neighbor (NN) hopping. In particular, the question concerning the nature of the ordered state is addressed. In a more general case of various concentration of both type of particles this problem was analyzed in Ref. 40.

In the limiting case of $t' \ll t$ one may expect that the checkerboard state is still the actual ground state of the FK model. In the opposite limit, when the hopping to the nearest sites can be neglected, the square lattice can be divided into two interpenetrating square sublattices with the lattice constant $\sqrt{2}$ times larger than the original one and with the axes rotated by 45°. Since the electrons do not hop between the sublattices, the system breaks up into two uncoupled, interpenetrating square lattices composed of NNN bonds. Each of these lattices is independently described by the FK Hamiltonian. Since both the sublattices are bipartite and both the subsystems are half–filled, the ions will arrange into checkerboard patterns in the ground state. Depending on the relative phase between the orderings in the sublattices, the resulting ground state of the whole system will have the form of vertical or horizontal stripes. Fig. 13 demonstrates these possibilities. In the large–U limit the threshold value of the ratio t'/t, that separates the ground states with ions forming the checkerboard and stripe patterns, can be determined using the mapping of the FK model onto the Ising one. In the antiferromagnetic Ising model with NN and NNN coupling the ground state is the simple antiferromagnet for $J'/J < 0.5$, where J and J' are the NN and NNN interactions, respectively. For $J'/J > 0.5$ the system minimizes the energy by ordering in alternate ferromagnetic rows of opposite spins.[41,42,43] Such spin configurations ("superantiferromagnetic") correspond to the ionic configurations of the FK model presented in Fig. 13. Since the ratio J'/J of Ising NN and NNN interactions is equal to $(t'/t)^2$ in the corresponding FK model, the threshold value of the NNN

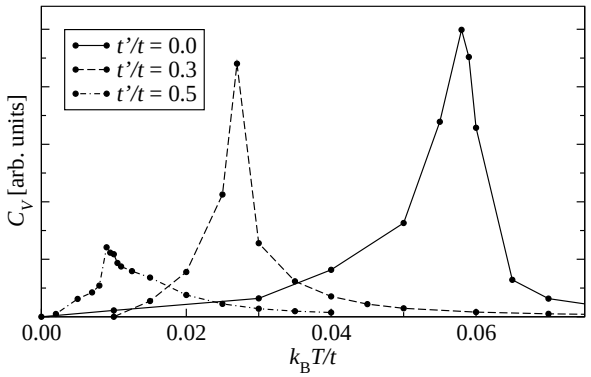


FIG. 14: Specific heat for $U/t = 1$ and $t'/t = 0,\ 0.3$ and 0.5.

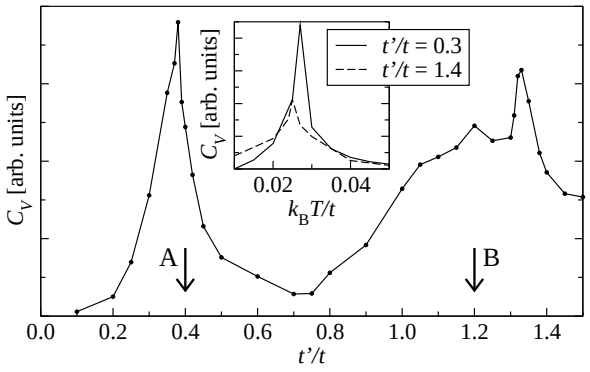


FIG. 15: Specific heat for $U/t = 1$ as a function of t'/t at $k_{\rm B}T/t = 0.02$. The arrows indicate values of t', for which $k_{\rm B}T/t = 0.02$ is the critical temperature of the phase transition from the checkerboard state (A) and from the stripe phase (B). The inset shows temperature dependence of the specific heat for $t'/t = 0.3$ and $t'/t = 1.4$.

hopping is given by $t'/t \simeq 0.71$. In Ref. 40 it has been shown that this result holds true up to fourth order in t/U. For weaker interaction this threshold ratio can be determined from a comparison of the ground state energy of both the checkerboard and stripe configurations. Our simulations indicate that the critical value of t'/t changes slightly with U, however, it always lies between 0.71 and 0.8.

B. Specific heat

Since the NNN hopping term introduces frustration, it reduces the temperature of the transition from the checkerboard to the disordered state (for $t'/t < 0.71$). In the strong interaction limit the dependence of the critical temperature on t'/t can be determined from results obtained for the corresponding Ising model with NNN interaction. For finite U/t the critical temperature can be identified from the position of the peak in the temperature dependence of the specific heat. Figure 14 presents results for $U/t = 1$. The critical temperature decreases with increasing t', going to zero for $t'/t \simeq 0.71$. At this point there is no long range order at any finite temperature. Then, the critical temperature increases with further increasing t'. In this regime the peak in the specific heat indicates the transition from the stripe configuration to the disordered state. For $t'/t \gg 1$ the nearest–neighbor hopping can be neglected and one ends up with the FK model on a square lattice with NN hopping integral t'. Therefore, according to the phase diagram presented in Fig. 8, in the limit $t'/t \to \infty$ (for a given U) the critical temperature goes to zero. Figure 15 shows how the specific heat depends on t'/t at temperature $k_{\rm B}T/t = 0.02$. This is a critical temperature for two different values of t': one for $t'/t = 0.4$, when in the low–temperature phase the ions form the checkerboard pattern, and the other for $t'/t = 1.2$, when stripes minimize the free energy at low temperature. As a result, the specific heat plotted as a function of t'/t has two maxima, as can be seen in Fig. 15. The left peak corresponds to the transition from the checkerboard state, whereas the right one to the transition from the stripe state. The widths of the peaks are connected with the effective sizes of the lattices. For large NNN hopping the lattice breaks up into two sublattices, which becomes decoupled in the limit of $t'/t \to \infty$ and the checkerboard pattern is formed in each of them independently. Therefore, the simulations are effectively carried out for two replicas of a system of halved size. As a result, the system is further away from the thermodynamic limit than in the case of small t' and the maximum of the specific heat is less sharp (see the inset in Fig. 15). The features seen at the top of the second maximum are connected with a rearrangement of the ions from two–dimensional structures to one–dimensional ones, as can be seen in the lowest row of Fig. 16. Figure 16 illustrates how the ionic configuration evolves from the checkerboard to stripe pattern with increasing amplitude of the NNN hopping. Due to the degeneracy of the ground state for $t'/t > 0.71$, showed in Figure 13, the evolution goes with equal probability through a state with vertical or horizontal stripes. Finally, for any finite temperature the system ends up in a disordered state.

C. Phase diagram

The determination of the full phase diagram of the FK model with NNN hoppings is a very CPU time consuming task due to the large number of free model parameters. Therefore, we have determined only a few points in order to qualitatively describe the dependence of the critical temperature on the ratio t'/t. Figure 17 shows the results for $U/t = 1$. This figure does not show the decrease of the critical temperature, when t' becomes very large. This is because we show the temperature in units of the NN hopping integral t. In the case of small NNN hopping, t is directly connected to the band width. However, when t' is very large, the band width is connected to t' rather then to t and $k_{\rm B}T_c/t'$, instead of $k_{\rm B}T_c/t$, would go to

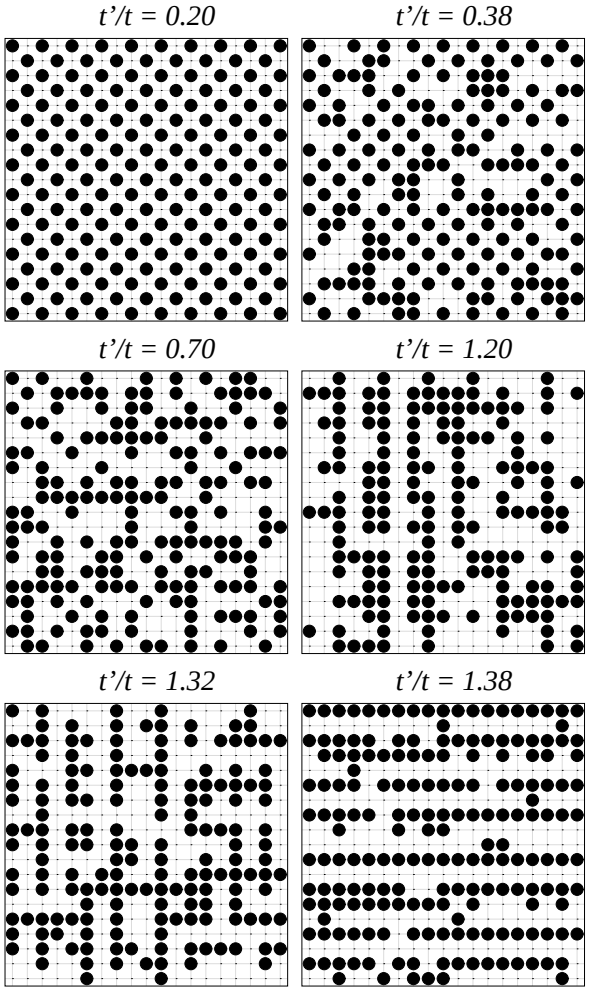


FIG. 16: Snapshots of ionic configurations for various NNN hopping amplitudes. The simulations were performed for $U/t = 1$ and $k_{\rm B}T/t = 0.02$.

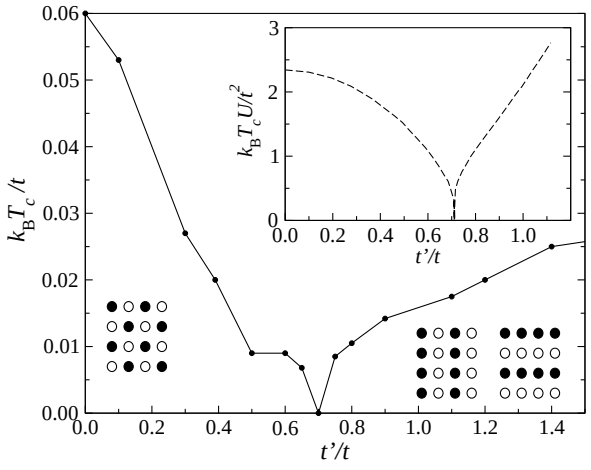


FIG. 17: Critical temperature as a function of t'/t for $U/t = 1$. The line connecting points is a guide for the eyes. The configurations indicate the ground states in given t'/t regimes. The inset shows the critical temperature in $U/t \to \infty$ limit.

zero when t' goes to infinity. The inset demonstrates the corresponding phase diagram in $U/t \to \infty$ limit obtained through mapping onto the NNN Ising model. Since the critical temperature goes to zero when U goes to infinity (for a given bandwidth), the temperature has been plotted as $k_{\rm B}TU/t^2$.

VI. DENSITY OF STATES

Since the electron distribution correlates with the ionic configuration, the formation of the checkerboard pattern results in a modification of the electronic density of states (DOS). The DOS at a given temperature can be obtained by averaging densities determined in each MC sweep. For weak electron–ion interaction at high temperature the electrons on average are almost unaffected by the ionic configurations and its DOS resembles that for free electrons on square lattice, except for the lack of the van Hove singularity (see Fig. 18c). As the temperature is lowered the ions form the checkerboard pattern and the electronic concentration decreases in sites that are occupied by the ions. As a result of this CDW order a gap opens in the DOS at the Fermi level (see Figs. 18a and 18b). The corresponding metal–insulator transition remains in accordance with the Mott picture.[44] The situation is different in the strong interaction regime. In this case, the electron–ion interaction almost completely forbids electrons from occupying sites that are already occupied by the ions. Therefore, even at high temperature the DOS averaged over the MC sweeps differs from the free electron DOS. At high enough temperature the Metropolis algorithm accepts every ionic configurations with probability almost equal to one. In other words, at high temperatures the ionic configurations are not affected by the electron–ion interaction and the ions are distributed randomly. In this regime, the FK model reduces itself to a model of free electrons in a random potential of disordered binary alloy. For large enough U there is a gap in the DOS, that does not change further with the increasing temperature (see Fig. 19c). When the temperature is lowered, this gap transforms itself into the CDW gap (Figs. 19a and 19b).

There is a significant difference in the temperature evolution of the DOS between the FK model and a CDW system with selfconsistently determined gap.[45] In the FK model the distance between the edges of the gap is constant when the temperature increases, but its depth as well as the high of the peaks decreases. It will be clearly visible in the proceeding section, where the spectral functions are presented. On the contrary, the width of the selfconsistently determined CDW gap decreases with increasing temperature, whereas its depth remains constant.

The DOS presented in Figs. 18 and 19 are obtained for 20×20 clusters. The question arises whether the fine structure seen in the DOS is a finite–size effect or is inherent to the FK model. The finite–size effects are es-

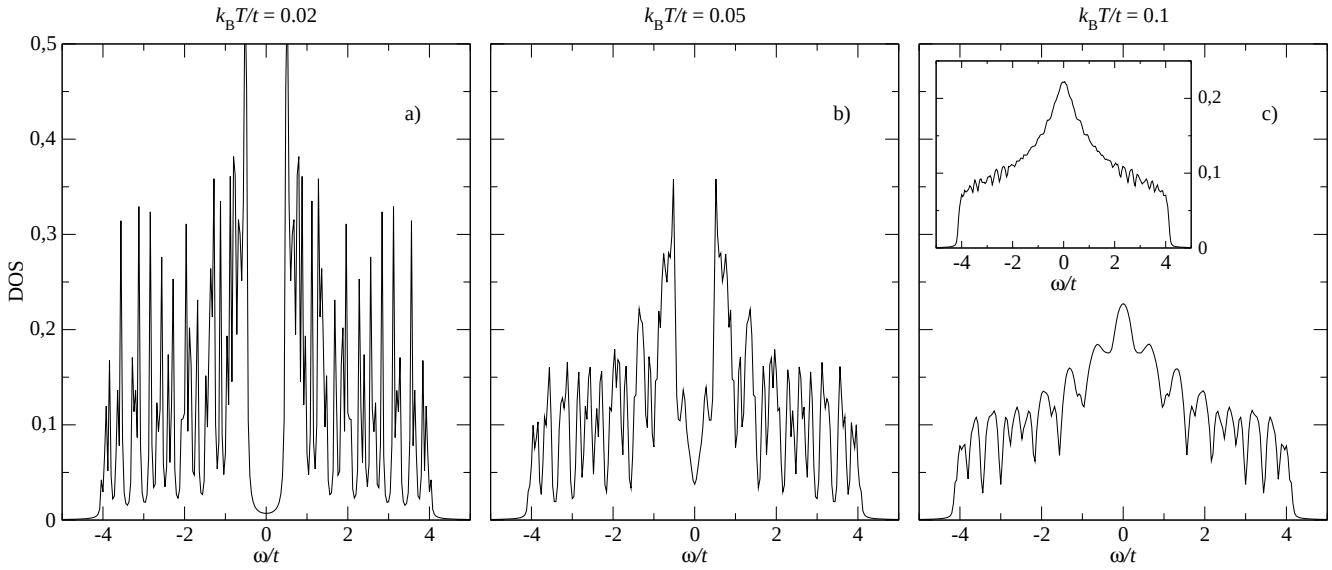


FIG. 18: Density of states for $U/t = 1$ at various temperatures. For temperatures T higher then $k_{\rm B}T/t = 0.1$ the DOS is almost the same as in panel c). The inset in panel c) shows the corresponding DOS for 40 × 40 cluster.

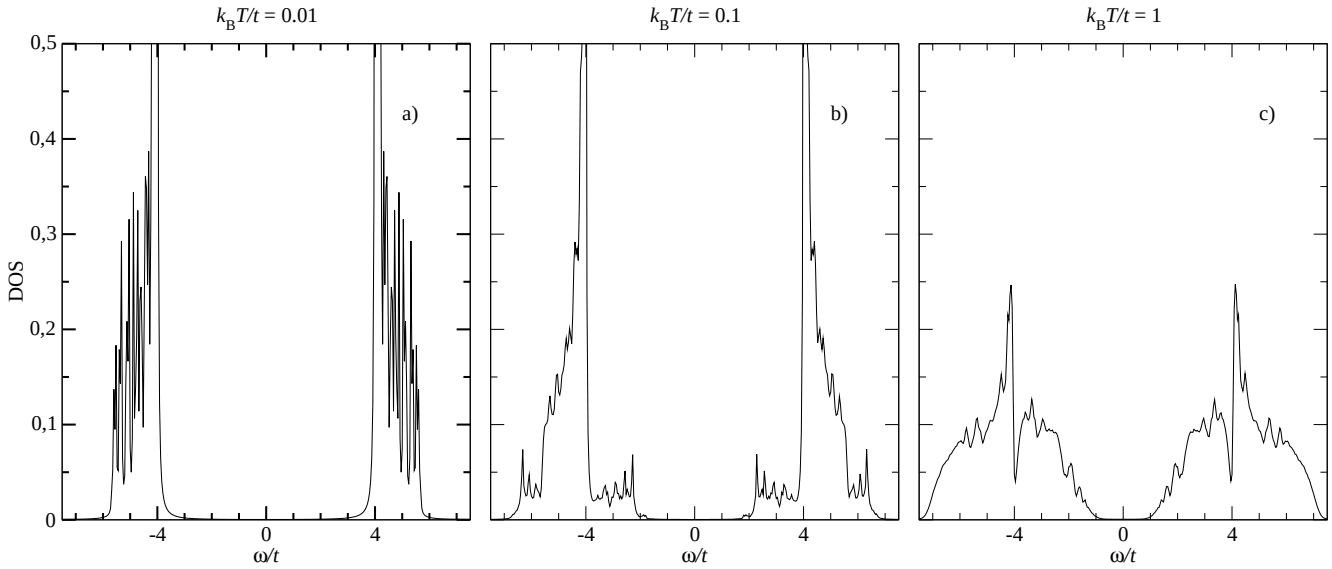


FIG. 19: Density of states for $U/t = 8$ at various temperatures. For temperatures T higher then $k_{\rm B}T/t = 1$ the DOS is almost the same as in panel c).

pecially important for small U. This drawback is visible in Fig. 18c, where the inset shows the DOS obtained for 40×40 cluster. In both cases of 20×20 and 40×40 clusters, the overall DOS resembles corresponding DOS for free electrons on square lattice. However, for the DOS obtained for 40×40 cluster is much more smooth, and therefore we attribute the fine structure to the finite size of the cluster. The DOS presented in Fig. 18c does not change with increasing temperature. This indicates that for $U/t = 1$ temperature $k_{\rm B}T/t = 0.1$ is high enough to treat the electrons described by the FK Hamiltonian as a free electron gas on a square lattice with diagonal disorder. Moreover, the interaction U is weak enough to neglect in this temperature regime the influence of averaged disorder and the actual DOS is almost the same as for free electrons on a square lattice.

On the other hand, when U increases, the DOS becomes much less dependent on the cluster size and the features that develop in the DOS can be attributed to the FK model itself. In order to confirm this assumption we compare DOS calculated for 20×20 cluster with delta function broadening $\eta = 0.02\,t$ and for 40×40 with $\eta = 0.005\,t$. Results are presented in Fig. 20. The smaller broadening used in the case of simulations on the larger cluster can uncover more details of the actual density of states. The differences between the DOS obtained

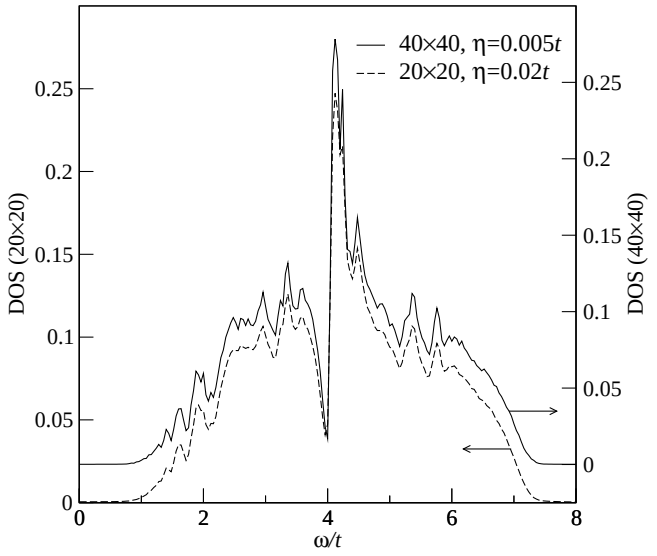


FIG. 20: Comparison of DOS obtained for 20×20 and 40×40 clusters with different delta function broadening. Note, that the right vertical axis is shifted in order to make the figure more legible. The presented results have been obtained for $U/t = 8$ at temperature $k_{\rm B}T/t = 1$, i.e., the same as in Fig. 19c.

for 20×20 and 40×40 clusters with the same broadening $\eta = 0.02t$ are within the linewidth. The results presented in Fig. 20 can be directly compared to results obtained using dynamical cluster approximation (see Fig. 6 in Ref. 28). When the size of the cluster increases from 1×1 (what corresponds to the dynamical mean–field approximation) to 8×8, some features start to develop in the DOS. The positions of these features are almost the same as in our MC calculations, however, they are less developed. In particular, it seems that the DOS at $\omega = \pm U/2$ vanishes in infinite system and narrow peaks are located at $|\omega|$ slightly larger than $U/2$. In Ref. 28, these peaks are attributed to the localization of electrons in four sites surrounding each site occupied by an ion. However, these features, as well as the overall density of states, do not change when the temperature increases. Moreover, the high–temperature density of states is exactly the same as the one for systems with random on–site binary disorder. Both the peak and the (pseudo)gap in the vicinity of $\pm U/2$ have been obtained within many approaches to disordered binary alloys.[46] This indicates that those peaks are rather connected with the strong interaction between electrons and randomly distributed ions.

VII. SPECTRAL PROPERTIES

The temperature and interaction dependence of the density of states is connected with the spectral properties of the FK model. Since at half filling there is no phase separation, the system is translation invariant and the ionic–configuration–averaged electronic Green function depends only on one momentum vector

$$\sum_{\boldsymbol{R}_i}\sum_{\boldsymbol{R}_j}\exp\left\{i\left(\boldsymbol{k}\cdot\boldsymbol{R}_i-\boldsymbol{k}'\cdot\boldsymbol{R}_j\right)\right\}\left\langle\mathcal{G}\left(\boldsymbol{R}_i,\boldsymbol{R}_j,z\right)\right\rangle = G\left(\boldsymbol{k},z\right)\delta\left(\boldsymbol{k}-\boldsymbol{k}'\right). \tag{12}$$

Here, $\mathcal{G}\left(\boldsymbol{R}_i,\boldsymbol{R}_j,z\right)=\left\{\left[z-\mathcal{H}(\mathcal{C})\right]^{-1}\right\}_{ij}$ is the real–space Green function for a given ionic configuration $\mathcal{C}$ and $\langle\ldots\rangle$ denotes averaging over the configurations. Then, the spectral function can be determined from the standard formula

$$A(\boldsymbol{k},\omega) = -\frac{1}{\pi}\mathrm{Im}\,G\left(\boldsymbol{k},\omega+i0^+\right). \tag{13}$$

Figure 21 shows the spectral weights corresponding to the DOS presented in Figures 18 and 19. In the relatively weak interaction regime ($U/t = 1$) at low temperature there is the CDW gap at $(0,\pi)$ and $(\pi/2,\pi/2)$ (Fig. 21a). The dispersion relation is very accurately described by $E_{\boldsymbol{k}} = \pm\sqrt{\left(\epsilon_{\boldsymbol{k}}-\mu\right)^2+U^2}$, where $\epsilon_{\boldsymbol{k}} = -t\left(\cos k_x+\cos k_y\right)$ is the energy of free electrons on a square lattice. With the increasing temperature the ionic disorder increases, destroying the checkerboard pattern. As a result, the spectral peaks gradually broadens up filling the gap (Fig. 21b). However, due to the weakness of the electron–ion interaction, this broadening is relatively small. Eventually, at high temperature the CDW gap disappears and the dispersion relation takes on the form of $\epsilon_{\boldsymbol{k}}$, that does not change with further increase of temperature (Fig. 21c). In the strong interaction regime ($U/t = 8$) at low temperature the dispersion relation can be described by the same formula, as for $U/t = 1$. In this case, however, the stronger interaction leads to almost equal spectral weights in the lower and upper subband and the band structure does not resemble that for free electrons any more (Fig. 21d). When the ionic disorder increases, additional bands appear, mainly around $(0,0)$ and (π,π) points (Fig. 21e). This effect is more visible in the corresponding DOS (Fig. 19b). These bands broaden up with farther increase of temperature and most of the spectral weight is transferred to them (Fig. 21f). Despite the broadening, at point $(0,\pi)$ there still exist flat parts of the bands, that are responsible for the peaks in the DOS at energy $\pm U/2$.

There exist some exact results for the mobile particles in the form of sum rules and the numerical results can be checked against them.[47,48] They give values of a few lowest spectral moments, defined by

$$\mu_n(\mathbf{k}) = \int_{\infty}^{\infty}\omega^n A(\mathbf{k},\omega). \tag{14}$$

Their values in the half–filling case are given by very simple expressions

$$\mu_0(\mathbf{k}) = 0,\quad \mu_1(\mathbf{k}) = \epsilon_{\mathbf{k}},\quad \mu_2(\mathbf{k}) = \epsilon_{\mathbf{k}}^2+\frac{U^2}{4}. \tag{15}$$

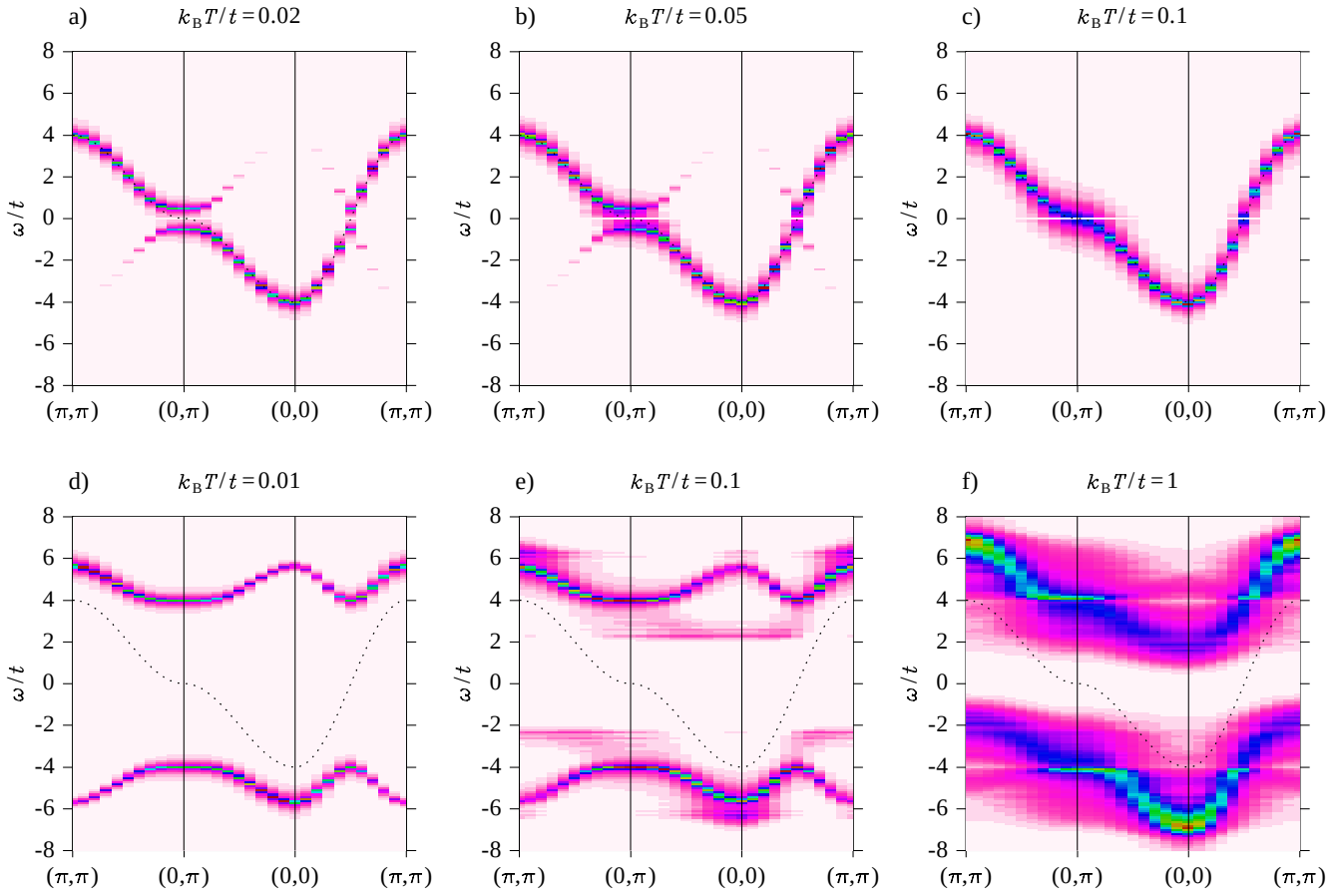


FIG. 21: (Color online) Spectral functions for $U/t = 1$ (upper row) and $U/t = 8$ (lower row) at various temperatures. The dotted line indicates dispersion of free electrons on the square lattice.

It is interesting that the same results are valid for the Hubbard model[49] and for the FK model in a nonequilibrium state.[47] Since in the proposed approach the FK Hamiltonian for a finite system is *exactly* diagonalized in each MC step, all these sum rules are *exactly* satisfied. As a result the sum rules are also satisfied for the spectral functions obtained in the whole MC run. However, the results for the moments are exact only if they are determined directly from the distribution of the eigenenergies in each MC step. The other approach, i.e., integrating ω^n with the spectral function obtained in the whole MC run, leads to a small error introduced by the broadening of the Dirac δ functions. The same holds true for the local moments,[47] where ω^n is integrated with the density of states.

VIII. SUMMARY

We have presented Monte Carlo analysis of half–filled FK model. In order to take into account both the classical and fermionic degrees of freedom, we have derived a modification of the classical Metropolis algorithm, where the interaction energy is replaced by free energy, calculated by numerical diagonalization of the FK Hamiltonian for a given ionic configuration. Such an approach is possible due to the absence of many–body interactions in the FK Hamiltonian. Although there is no many–body term in the Hamiltonian, averaging over ionic configurations ("annealing") leads to many–body effects in the FK model. As a result, the FK model possesses a rich phase diagram. The simulations presented in this paper concern the case of $\rho_i = \rho_e = 0.5$, i.e., the case where the ground state is known to be the checkerboard ionic configuration. Our results illustrate how the system reaches this state when the temperature is lowered. It is known, that in the strong interaction limit the FK model maps onto the Ising model, and therefore the phase transition to the ordered state is of second order. There is no such a rigorous result for weakly interacting 2D FK model. Our simulations indicate the presence of a first–order phase transition in this regime. However, the precise determination of the critical value of the interaction, below which the phase transition is of first order, requires extensive

simulations, mostly in order to perform the finite–size scaling.

Additionally, we have shown that the order parameter decreases unusually with increasing temperature in this regime. A departure from the Ising–type temperature dependence of the order parameter has recently been demonstrated also in infinite dimensions.[37]

Performing the MC simulations for various interaction strengths and at various temperatures, we have constructed the phase diagram for half–filled FK model. It was shown, that the boundary line, separating the ordered (checkerboard) and disordered phases, determined from positions of the peaks in the specific heat and in the CDW susceptibility coincides with the one obtained from the opening of a gap in the electronic DOS. The phase diagram has also been determined in the presence of NNN hopping. It was shown, that there is a point (for $t'/t \approx 0.7 \div 0.8$, depending on the interaction strength) at which no long range order exists at any finite temperature. For larger t' the ions at low temperate form horizontal or vertical stripes.

The electronic DOS and spectral functions have been determined for a wide range of the interaction strength. In the large–U limit, the distribution of electrons strongly depends on the ionic configuration. As a result, the CDW gap develops in the DOS at low temperatures. At high temperatures, the ions are distributed randomly over the lattice sites and the electronic DOS is the same as in a free electron system with a diagonal disorder. On the other hand, in the weak interaction regime the electrons are hardly affected by the ions, and averaging over the ionic configurations leads to the same band structure as for free electrons on a square lattice. We have shown, that the proposed approach give both the electronic DOS and spectral functions in a good agreement with that obtained with use of much more elaborated DCA method, whereas the computational effort is much lower.

The present paper demonstrated how the MC approach can be used to describe the formation of the checkerboard order in the half–filled FK model. It is also possible to use this method to analyze the FK model away from half–filling, where inhomogeneous states are expected to minimize the free energy at low enough temperatures. The MC method would be particularly useful to describe phases with irregular ionic configurations, e.g., phase separation, which are difficult to analyze analytically. Preliminary result in this area are presented in Ref. 31. Another area where the Monte Carlo study of the Falicov–Kimball may be particularly useful, includes nonbipartite lattices. In this case, the checkerboard pattern cannot be formed even at half–filling, and the model is expected to exhibit a strong frustration. This issue is under current investigation.[32]

Acknowledgments

The authors acknowledge stimulating discussions with Jim Freericks, Romuald Lemański, Marcin Mierzejewski, and Stanisław Robaszkiewicz. The authors also acknowledges support from the Polish Ministry of Education and Science under Grant No. 1 P03B 071 30.

* Electronic address: maciek@phys.us.edu.pl

1 J. Hubbard, Proc. R. Soc. London A **276**, 238 (1963); *ibid.* **281**, 401 (1964).
2 J. G. Bednorz and K. A. Müller, Z. Phys. B **64**, 188 (1986).
3 P. W. Anderson, Science **235**, 1196 (1987).
4 E.H. Lieb and F.Y. Wu, Phys. Rev. Lett. **20**, 1445 (1968).
5 Y. Nagaoka, Phys. Rev. **147**, 392 (1966).
6 A. Georges and G. Kotliar, Phys. Rev. B **45**, 6479 (1992).
7 M. Jarrell, Phys. Rev. Lett. **69**, 168 (1992).
8 L.M. Falicov and J.C. Kimball, Phys. Rev. Lett. **22**, 997 (1969).
9 T. Kennedy and E.H. Lieb, Physica A **138**, 320 (1986).
10 E.H. Lieb, Physica A **140**, 240 (1986).
11 J.K. Freericks and R. Lemański, Phys. Rev. B **61**, 13438 (2000).
12 J.K. Freericks, E.H. Lieb, and D. Ueltschi, Phys. Rev. Lett. **88**, 106401 (2002).
13 B.M. Letfulov and J.K. Freericks, Phys. Rev. B **66**, 033102 (2002).
14 P. Farkašovský, Phys. Rev. B **60**, 10776 (2000).
15 J.K. Freericks, Ch. Gruber, and N. Macris, Phys. Rev. **B** 60 1617 (1999); **53**, 16189 (1996).
16 R. Lemański, J.K. Freericks, and G. Banach, Phys. Rev. Lett. **89**, 196403 (2002).
17 R. Lemanski, J.K. Freericks and G. Banach, J. Stat. Phys. **116**, 699 (2004).
18 K. Haller and T. Kennedy, J. Stat. Phys. **102**, 15 (2001).
19 G.I. Watson and R. Lemański, J. Phys. Condens. Matter **7**, 9521 (1995).
20 P. de Vries, K. Michielson, and H. De Raedt, Z. Phys. B **92**, 353 (1993).
21 J.K. Freericks and L.M. Falicov, Phys. Rev. B **41**, 2163 (1990).
22 J.K. Freericks, Phys. Rev. B **47**, 9263 (1993).
23 Ch. Gruber, D. Ueltschi, and J. Jędrzejewski, J. Stat. Phys. **76**, 125 (1994).
24 R. Łyżwa, Physica A **192**, 231 (1993).
25 U. Brandt and C. Mielsch, Z. Phys. B: Condens. Matter **75**, 365 (1989), **79**, 295 (1990); **82**, 37 (1991).
26 P.G.J.van Dongen and D. Vollhardt, Phys. Rev. Lett. **65**, 1663 (1990).
27 W. Metzner and D. Vollhardt, Phys. Rev. Lett. **62**, 324 (1989).
28 M.H. Hettler, A.N. Tahvildar–Zadeh, M. Jarrell, T. Pruschke, and H.R. Krishnamurthy, Phys. Rev. B **58**, R7475 (1998).
29 M.H. Hettler, M. Mukherjee, M. Jarrell, and H. R. Krishnamurthy, Phys. Rev. B **61**, 12739 (2000).
30 P. Farkašovský, Z. Phys. B **102**, 91 (1997).
31 M.M. Maśka and K. Czajka, phys. stat. sol. (b) **242**, 479

(2005).
[32] K. Czajka and M.M. Maśka, Physica B (*in press*).
[33] M.M. Maśka and K. Czajka, Physica B, **359-361**, 693 (2005).
[34] N. Metropolis, A. Rosenbluth, M. Rosenbluth, A. Teller and E. Teller, J. Chem. Phys. **21**, 1087 (1953).
[35] A similar approximation has been used, e.q., in: J. Schliemann, J. König, and A.H. MacDonald, Phys. Rev. B **64**, 165201 (2001).
[36] K. Binder and D.W Heermann, *Monte Carlo Simulation in Statistical Physics: An Introduction*, Springer, Heidelberg (2002); D. Landau and K. Binder, *A Guide to Monte Carlo Simulations in Statistical Physics*, Cambridge University Press, Cambridge, 2005.
[37] Ling Chen, J.K. Freericks, and B.A. Jones Phys. Rev. B **68**, 153102 (2003).
[38] M.S.S. Challa, D.P. Landau, and K. Binder, Phys. Rev. B **34**, 1841 (1986).
[39] P.G.J. van Dongen, Phys. Rev. B **45**, 2267 (1992).
[40] J. Wojtkiewicz, `cond--mat/0310043`.
[41] D.P. Landau, Phys. Rev. B **21**, 1285 (1980).
[42] D.P. Landau and K. Binder, Phys. Rev. B **31**, 5946 (1985).
[43] J.L. Morán–López, F. Aguilera–Granja, and J.M. Sanchez, Phys. Rev. B **48**, 3519 (1993).
[44] N. F. Mott, Rev. Mod. Phys. **40**, 677 (1968); *Metal Insulator Transitions* (Taylor & Francis, London, 1974).
[45] G. Grüner *Density Waves in Solids* (Addison-Wesley, Reading, MA, 1994).
[46] A.E. Carlsson and P.A. Fedders, Phys. Rev. B **34**, 3567 (1986); P. Dean, Rev. Mod. Phys. **44**, 127 (1972).
[47] J.K. Freericks, V.M. Turkowski, and V. Zlatić, Phys. Rev. B **71**, 115111 (2005).
[48] V.M. Turkowski and J.K. Freericks, cond-mat/0511063.
[49] S.R. White, Phys. Rev. B **44**, 4670 (1991).